

THE OFFICIAL MAGAZINE OF THE OCEANOGRAPHY SOCIETY

# Oceanography

## CITATION

Thangaprakash, V.P., M.S. Girishkumar, K. Suprit, N. Suresh Kumar, D. Chaudhuri, K. Dinesh, A. Kumar, S. Shivaprasad, M. Ravichandran, J.T. Farrar, R. Sundar, and R.A. Weller. 2016. What controls seasonal evolution of sea surface temperature in the Bay of Bengal? Mixed layer heat budget analysis using moored buoy observations along 90°E. *Oceanography* 29(2):202–213, <http://dx.doi.org/10.5670/oceanog.2016.52>.

## DOI

<http://dx.doi.org/10.5670/oceanog.2016.52>

## COPYRIGHT

This article has been published in *Oceanography*, Volume 29, Number 2, a quarterly journal of The Oceanography Society. Copyright 2016 by The Oceanography Society. All rights reserved.

## USAGE

Permission is granted to copy this article for use in teaching and research. Republication, systematic reproduction, or collective redistribution of any portion of this article by photocopy machine, reposting, or other means is permitted only with the approval of The Oceanography Society. Send all correspondence to: [info@tos.org](mailto:info@tos.org) or The Oceanography Society, PO Box 1931, Rockville, MD 20849-1931, USA.

# What Controls Seasonal Evolution of Sea Surface Temperature in the Bay of Bengal?

Mixed Layer Heat Budget Analysis Using Moored Buoy Observations Along 90°E

By V.P. Thangaprakash,  
M.S. Girishkumar, K. Suprit,  
N. Suresh Kumar, Dipanjan Chaudhuri,  
K. Dinesh, Ashok Kumar,  
S. Shivaprasad, M. Ravichandran,  
J. Thomas Farrar, R. Sundar,  
and Robert A. Weller

**ABSTRACT.** Continuous time-series measurements of near surface meteorological and ocean variables obtained from Research Moored Array for African-Asian-Australian Monsoon Analysis and Prediction (RAMA) moorings at 15°N, 90°E; 12°N, 90°E; and 8°N, 90°E and an Ocean Moored buoy Network for Northern Indian Ocean (OMNI) mooring at 18°N, 90°E are used to improve understanding of air-sea interaction processes and mixed layer (ML) temperature variability in the Bay of Bengal (BoB) at seasonal time scales. Consistent with earlier studies, this analysis reveals that net surface heat flux primarily controls the ML heat balance. The penetrative component of shortwave radiation plays a crucial role in the ML heat budget in the BoB, especially during the spring warming phase when the ML is thin. During winter and summer, vertical processes contribute significantly to the ML heat budget. During winter, the presence of a strong barrier layer and a temperature inversion (warmer water below the ML) leads to warming of the ML by entrainment of warm subsurface water into the ML. During summer, the barrier layer is relatively weak, and the ML is warmer than the underlying water (i.e., no temperature inversion); hence, the entrainment cools the mixed layer. The contribution of horizontal advection to the ML heat budget is greatest during winter when it serves to warm the upper ocean. In general, the residual term in the ML heat budget equation is quite large during the ML cooling phase compared to the warming phase when the contribution from vertical heat flux is small.

*Photo credit: N. Suresh Kumar*



## INTRODUCTION

Sea surface temperature (SST) in the Bay of Bengal (BoB) strongly influences the spatiotemporal evolution of precipitation over the Indian subcontinent (e.g., Shenoi et al., 2002). In general, BoB SST is greater than 28°C throughout the year, except during winter, and this temperature is generally considered as a threshold for atmospheric deep convection (Shenoi et al., 2002). A slight SST variation in regions of high mean SST, particularly in basins like the BoB, can result in a strong atmospheric circulation response (Palmer and Mansfield, 1984). In order to forecast the spatiotemporal evolution of precipitation patterns over the Indian subcontinent and nearby landmass, it is imperative to represent BoB SST accurately in the oceanic component of coupled general circulation models (Sengupta et al., 2001; Sharmila et al., 2013). In this paper, we use unique in situ observations and satellite data to examine some of the factors driving SST variability in the BoB.

The mixed layer (ML) is defined as the uppermost layer of the ocean where temperature, salinity, and density ( $\sigma_t$ ) are vertically uniform due to turbulent mixing associated with air-sea exchange of momentum and heat flux (Kara et al., 2000). However, in regions like the BoB, large freshwater input to the near-surface layer from intense monsoon precipitation and river discharge leads to a shallow, salt-stratified ML above the deeper isothermal layer (Shetye et al., 1996; Rao and Sivakumar, 2003; Thadathil et al., 2007). The layer between the shallow salt-stratified ML and the isothermal layer is called the barrier layer (Lukas and Lindstrom, 1991; Shetye et al., 1996; Shenoi et al., 2002; Rao and Sivakumar, 2003; Thadathil et al., 2007; Sengupta et al., 2007; Girishkumar et al., 2011). The barrier layer is often accompanied by a temperature inversion, a situation in which cool water overlies warm water (Thadathil et al., 2002; Sengupta et al., 2007; Girishkumar et al., 2013). Figure 1 illustrates the ML, the isothermal layer, the

barrier layer, and a temperature inversion.

Many attempts have been made to understand the seasonal variability of SST in the BoB by estimating the ML heat budget using observations (Rao and Sivakumar 2000; Sengupta and Ravichandran, 2001; Sengupta et al., 2001, 2002; Shenoi, 2002; Parampil et al., 2010; Neethu et al., 2012; Girishkumar et al., 2013) and models (Prasad, 2004; Boyer Montégut et al., 2007; Chowdary et al., 2015). All of these studies highlight the importance of net surface heat flux and near-surface salinity stratification for the evolution of SST variability in the BoB (Rao and Sivakumar, 2000; Sengupta et al., 2001, 2002; Sengupta and Ravichandran, 2001; Shenoi et al., 2002; Boyer Montégut et al., 2007; Parampil et al., 2010). These studies also suggest that the barrier layer and temperature inversion play significant roles in the evolution of SST in the BoB (Shenoi et al., 2002; Prasad, 2004; Boyer Montégut et al., 2007; Sengupta et al., 2007; Girishkumar et al., 2013; Nagura et al., 2015). Some studies highlight the importance of heat flux from the subsurface to the ML, due to vertical processes, on the evolution

of SST in the BoB (Prasad, 2004; Boyer Montégut et al., 2007; Girishkumar et al., 2013; Nagura et al., 2015).

Here, we use long-term, high-quality in situ meteorological and ocean data to estimate the ML heat budget and examine the seasonal variability of air-sea interaction processes and ML temperature variability in the BoB. Few studies have analyzed the ML heat budget using moored buoy observations in the BoB (Neethu et al., 2012; Girishkumar et al., 2013), and all of these analyses were restricted to a single mooring for a shorter duration (approximately four months). The primary objective of this study is to understand the meridional variation of relative contributions of air-sea fluxes, ocean dynamics, and seasonal warming and cooling and how it affects the evolution of SST in the BoB. To achieve this goal, we use high-quality, in situ observations from a buoy network along 90°E (Figure 2a) that includes three Research Moored Array for African-Asian-Australian Monsoon Analysis and Prediction (RAMA) moorings at 15°N, 90°E; 12°N, 90°E; and 8°N, 90°E (McPhaden et al., 2009) and one additional mooring at 18°N, 90°E from

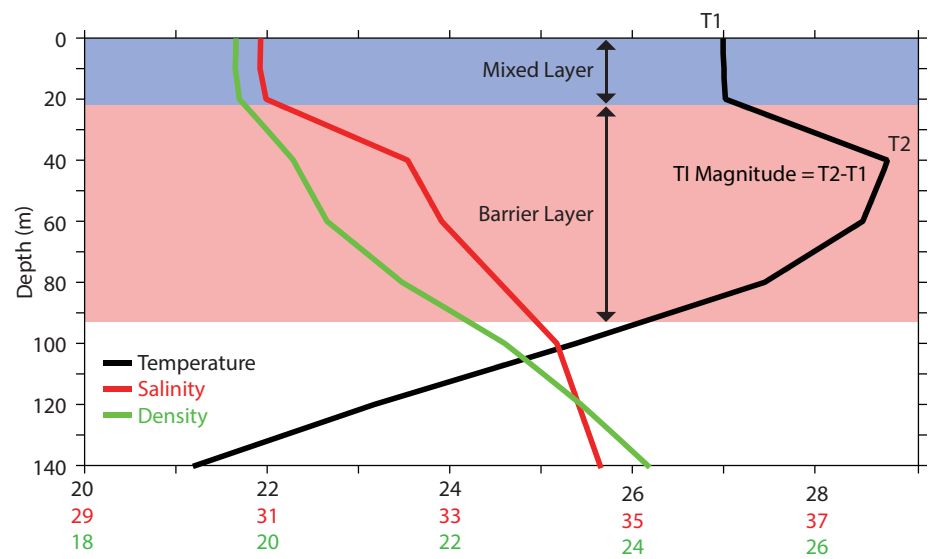


**FIGURE 1.** Example of a mixed layer (blue shaded region), a barrier layer (red shaded region), and an isothermal layer (sum of mixed layer and barrier layer) estimated from temperature (°C, black), salinity (psu, red), and  $\sigma_t$  ( $\text{kg m}^{-3}$ , green) data from the Research Moored Array for African-Asian-Australian Monsoon Analysis and Prediction (RAMA) buoy at 15°N, 90°E on January, 14, 2009, in the Bay of Bengal. The magnitude of the temperature inversion (TI) is defined as the difference between sea surface temperature 1 m below the buoy (T1) and the maximum temperature (T2) in the barrier layer as observed in the vertical temperature profile.



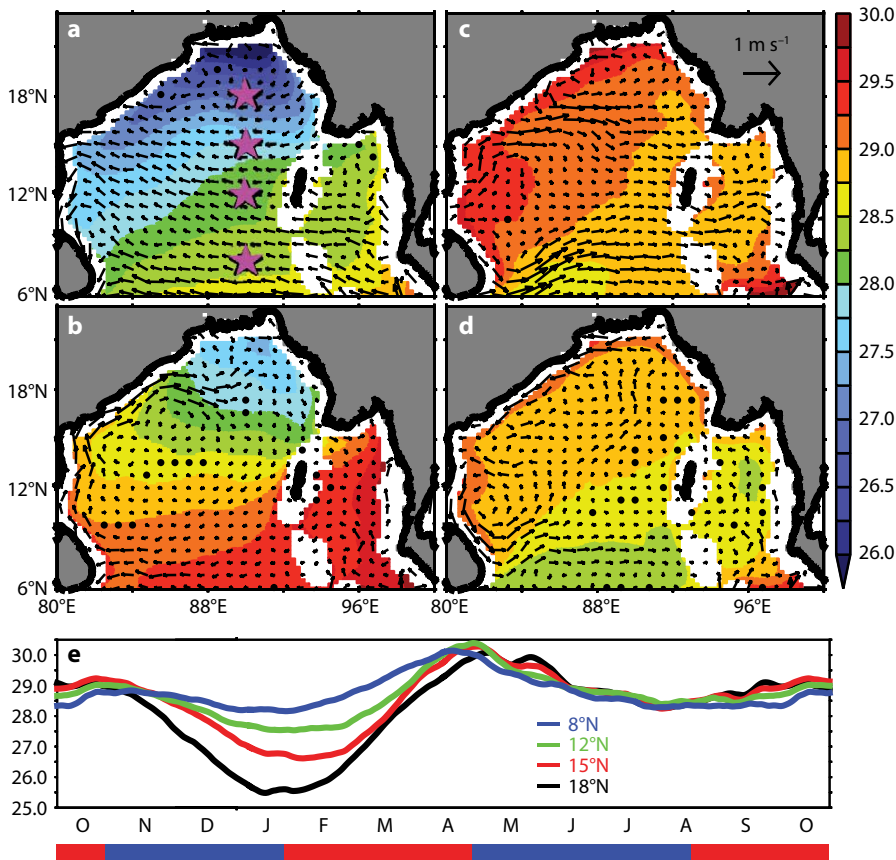


**FIGURE 2.** Seasonal averages (a) November 1 to January 31, (b) February 1 to May 10, (c) May 11 to August 15, and (d) August 16 to October 31 of daily WindSAT Microwave Optimum Interpolation Sea Surface Temperature (OISST; °C; shaded) climatology (1997–2015) and QuikSCAT wind vector ( $\text{m s}^{-1}$ ) climatology (2000–2009). (e) Temporal evolution of OISST (°C) climatology (1997–2015) at the four buoy locations ( $18^\circ\text{N}$ ,  $15^\circ\text{N}$ ,  $12^\circ\text{N}$ ,  $8^\circ\text{N}$ ), marked as pink stars in (a) in the Bay of Bengal (10-day running mean is applied). The color bar below the graph in (e) indicates cooling (blue) and warming periods (red).

the Ocean Moored buoy Network for Northern Indian Ocean (OMNI; BD09; Venkatesan et al., 2013).

## DATA AND METHODOLOGY

The present study is based on mooring observations during the period 2007–2015. Tables 1 and 2 summarize the data availability and analysis period of the moorings. Because the temperature and salinity measurements are discrete in the vertical (Table 2), the data were linearly interpolated to 1 m intervals. We considered temperature and salinity measurements at 1 m as SST and sea surface salinity (SSS), respectively.

We estimated the ML depth (MLD) as the depth at which the density is equal to the sea surface density plus an increment equivalent to the density change that would be associated with some prescribed change in temperature,  $\Delta T$  (Sprintall and Tomczak, 1992; Rao and Sivakumar, 2003). Therefore, the base of the ML is the depth at which

$$\sigma_{t(z=h)} = \sigma_{t(z=0)} + \Delta\sigma_t,$$

where

$$\Delta\sigma_t = \sigma(T_0 + \Delta T, S_0, P_0) - \sigma(T_0, S_0, P_0) \approx \frac{\partial\sigma_t}{\partial T}\Delta T,$$

$\sigma_{t(z=0)}$  is the surface  $\sigma_t$ ,  $\Delta T$  is the desired temperature criterion described below,

and  $\frac{\partial\sigma_t}{\partial T}$  is the coefficient of thermal

expansion evaluated using SST ( $T_0$ ) and SSS ( $S_0$ ) (Kara et al., 2000). Earlier studies suggest that  $\Delta T = 0.8^\circ\text{C}$  is a more reliable temperature criterion for MLD, and this has been adopted for the calculation

**TABLE 1.** Periods of data collection used for this study at the different mooring locations in the Bay of Bengal.

Moorings	Mooring locations	Buoy data period used for this study
OMNI-BD09	$18^\circ\text{N}$ , $90^\circ\text{E}$	February, 1, 2015, to November 13, 2016
WHOI	$18^\circ\text{N}$ , $90^\circ\text{E}$	December 3, 2014, to January 13, 2016 (downwelling longwave radiation only)
RAMA	$15^\circ\text{N}$ , $90^\circ\text{E}$	November 1, 2008, to July 31, 2010 November 15, 2013, to February 28, 2015
	$12^\circ\text{N}$ , $90^\circ\text{E}$	November 15, 2007, to February 28, 2009
	$08^\circ\text{N}$ , $90^\circ\text{E}$	November 1, 2010, to May 31, 2013

**TABLE 2.** Summary of measurement at RAMA and OMNI moorings in the Bay of Bengal.

Network and Location	Variables
RAMA $15^\circ\text{N}$ , $90^\circ\text{E}$ ; $12^\circ\text{N}$ , $90^\circ\text{E}$ ; $8^\circ\text{N}$ , $90^\circ\text{E}$	<ul style="list-style-type: none"> <li>Temperature: 1, 10, 13, 20, 40, 43, 60, 80, 100, 120, 140, 180, 300, and 500 m depths</li> <li>Salinity: 1, 10, 20, 40, 60, 100, and 120 m depths</li> <li>Currents: At fixed depths of 10 m and 40 m at <math>15^\circ\text{N}</math> and 10 m at <math>12^\circ\text{N}</math> and <math>8^\circ\text{N}</math></li> <li>Meteorological measurements: downwelling shortwave and downwelling longwave radiation, winds (4 m), SST (at 1 m), air temperature (at 3 m), relative humidity (at 3 m), and barometric pressure</li> <li>Net longwave radiation from TropFlux (Kumar et al., 2012) was used at all buoy locations except <math>15^\circ\text{N}</math>, <math>90^\circ\text{E}</math></li> </ul>
BD09 $18^\circ\text{N}$ , $90^\circ\text{E}$	<ul style="list-style-type: none"> <li>Temperature: 1, 10, 15, 20, 30, 50, 75, 100, 200, and 500 m depths</li> <li>Salinity: 1, 10, 15, 20, 30, 50, 75, 100, 200, and 500 m depths</li> <li>150 kHz acoustic Doppler current profiler (downward facing) measuring current profiles at an interval of 5 m from the near surface to 105 m depth</li> <li>Meteorological: Downwelling shortwave radiation, air pressure, air temperature, humidity, wind speed, and direction (at 3 m)</li> </ul>

of MLD in this study (Kara et al., 2000; Du et al., 2005; Neethu et al., 2012). The isothermal layer depth (ILD) is defined as the depth where the temperature is 0.8°C lower than SST. This definition of ILD is consistent with the variable density criterion so that in the absence of salinity variation, MLD and ILD are identical. Barrier layer thickness is defined as the difference between MLD and ILD. By definition, a temperature inversion occurs when SST is lower than water temperature at depth by 0.1°C (Figures 1 and 3; Thadathil et al., 2002; Girishkumar et al., 2013).

To investigate the processes that control seasonal evolution of SST, we examined the surface ML heat budget using

$$\rho C_p h \frac{\partial T}{\partial t} = Q_{net} - \rho C_p h \left[ \left( u \frac{\partial T}{\partial x} + v \frac{\partial T}{\partial y} \right) + H \left( W_h + \frac{dh}{dt} \right) \frac{(T - T_h)}{h} \right] + \text{Residual}, \quad (1)$$

where  $Q_{net}$  is the net surface heat flux and

$$Q_{net} = Q_{shortwave} - (Q_{pen} + Q_{longwave} + Q_{latent} + Q_{sensible}),$$

$Q_{shortwave}$  = net shortwave radiation,  $Q_{pen}$  = shortwave radiation that penetrates below the ML,  $Q_{longwave}$  = net longwave radiation,  $Q_{latent}$  = latent heat flux, and  $Q_{sensible}$  = sensible heat flux. The individual terms in Equation 1 represent (from left to right): ML heat storage, net surface heat flux ( $Q_{net}$ ), horizontal advection, heat flux due to vertical processes, and the residual. Here,  $T$  is temperature (°C) averaged over the ML,  $\rho$  is the density of seawater (1,024 kg m<sup>-3</sup>),  $C_p$  is the specific heat capacity of seawater (3,993 J kg<sup>-1</sup> K<sup>-1</sup>),  $t$  is time (in days),  $h$  is MLD (m),  $W_h$  is vertical advection (m day<sup>-1</sup>), and  $H$  is the Heaviside step function (its value is zero when  $(W_h + dh/dt)$  is negative [no vertical heat flux] and unity otherwise).  $T_h$  is the temperature 5 m below the MLD, representing temperature just below the ML base (Du et al., 2005; Girishkumar et al., 2013).

The vertical process term consists of the combined effect of both entrainment velocity and vertical advection

( $W_h$  in m day<sup>-1</sup>), where the entrainment velocity is estimated by the rate of change in the MLD ( $dh/dt$  in m day<sup>-1</sup>). Following earlier studies,  $W_h$  is estimated from the rate of change of a representative isotherm in the thermocline (McPhaden, 1982; Rao and Sivakumar, 2000; Girishkumar et al., 2013). Girishkumar et al. (2013) and Neethu et al. (2012) used the rate of change of the depth of the 23°C isotherm to estimate  $W_h$  in the BoB, and the same is adopted for this study. In order to test the sensitivity of the vertical process

term, it is estimated with different isotherms from 20°C to 25°C (Figure 4). The root-mean-square difference (RMSD) between the 23°C and 25°C isotherms for monthly vertical processes is found to be 8 W m<sup>-2</sup>, and between the 20°C and 23°C isotherms it is 5 W m<sup>-2</sup>. We did not consider the vertical eddy diffusivity term in Equation 1 because of the uncertainty involved in the determination of the vertical eddy diffusivity coefficient.

Ideally, current and temperature averaged over the MLD are used to estimate

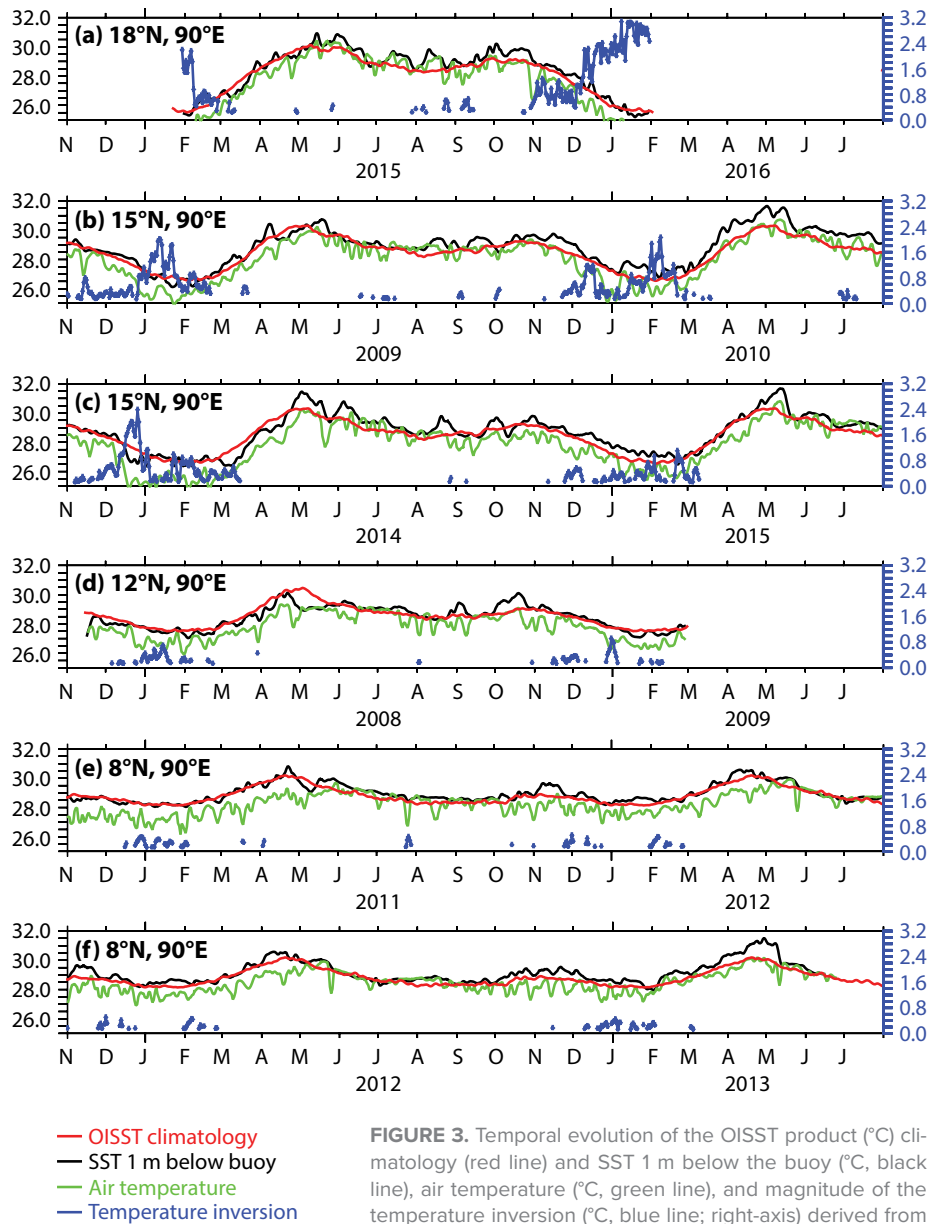


**FIGURE 3.** Temporal evolution of the OISST product (°C) climatology (red line) and SST 1 m below the buoy (°C, black line), air temperature (°C, green line), and magnitude of the temperature inversion (°C, blue line; right-axis) derived from the Bay of Bengal moorings during the study period. (a) 18°N, 90°E. (b,c) 15°N, 90°E. (d) 12°N, 90°E. (e,f) 8°N, 90°E. All of the time series variables except magnitude of the temperature inversion are smoothed with a three-day running mean.

the horizontal advection term in the ML heat budget equation. However, due to the lack of vertical resolution in the velocity data, particularly at the RAMA mooring locations, the currents at 10 m depth are used as a proxy for ML averaged current. This representation is justified by comparing ML averaged zonal and meridional currents with 10 m currents from the BD09 mooring. The statistical comparison shows good agreement between the 10 m currents and the ML averaged currents, with a correlation coefficient of 0.87 and an RMSD of 0.09 m s<sup>-1</sup> for the

zonal current and 0.90 and 0.08 m s<sup>-1</sup> for the meridional current, respectively.

We assume that the temperature is approximately uniform from the surface to the base of the ML. Hence, the horizontal gradient of temperature ( $\partial T/\partial x$  and  $\partial T/\partial y$ ) is estimated from the Advanced Microwave Scanning Radiometer for EOS (AMSR-E), AMSR-2, Tropical Rainfall Measuring Mission (TRMM) Microwave Imager (TMI), and the WindSAT Microwave Optimum Interpolation Sea Surface Temperature product (OISST) with 0.25° grid spacing (~25 km)

(Gentemann et al., 2003) following the method of Vialard et al., (2008). A statistical comparison between OISST and ML temperature shows reasonably good agreement, with a correlation of 0.96 and an RMSD of 0.34°C at all the mooring locations used in this study.

The Coupled Ocean-Atmosphere Response Experiment (COARE, Version 2.0) bulk flux algorithm (Fairall et al., 2003) is used to estimate turbulent heat fluxes from the ocean (latent and sensible heat fluxes). Following the methodology of Dickey et al. (1994), downwelling longwave radiation obtained from a mooring is used to estimate net longwave radiation. The RAMA buoys at 12°N and 8°N do not have longwave radiation sensors; hence, net longwave radiation from TropFlux is used in this study (Praveen Kumar et al., 2012). Further, downwelling longwave radiation measurements from the BD09 mooring show bias throughout the study period, and they have been replaced with measurements from the Woods Hole Oceanographic Institution (WHOI) mooring at 17.98°N, 89.45°E. An albedo correction of 0.945 is applied to downwelling shortwave radiation measured at the buoy to estimate net surface shortwave radiation.

Following Sengupta et al. (2002) and Parampil et al. (2010), the amount of shortwave radiation that penetrates below the ML base is estimated using  $Q_{pen} = Q_{shortwave} * (1 - \alpha)^{-h/\zeta}$ , where  $\alpha = 0.58$  is the fraction of red and infrared part of shortwave radiation, which is generally absorbed within the upper 2 m of the water column.  $\zeta$  is the attenuation depth, and it is calculated from Moderate Resolution Imaging Spectroradiometer (MODIS)-Aqua monthly composite chlorophyll-*a* data using the expression  $\zeta = 1/(0.027+(0.0518 * \text{chlorophyll}^{0.428}))$  (Morel, 1988). On average, attenuation depths at all the buoy locations during the study period are found to be ~20 m (minimum in the northern bay [18 m] and maximum in the south [21 m]), which indicates that approximately 25%, 15%, and 9% of shortwave radiation penetrates

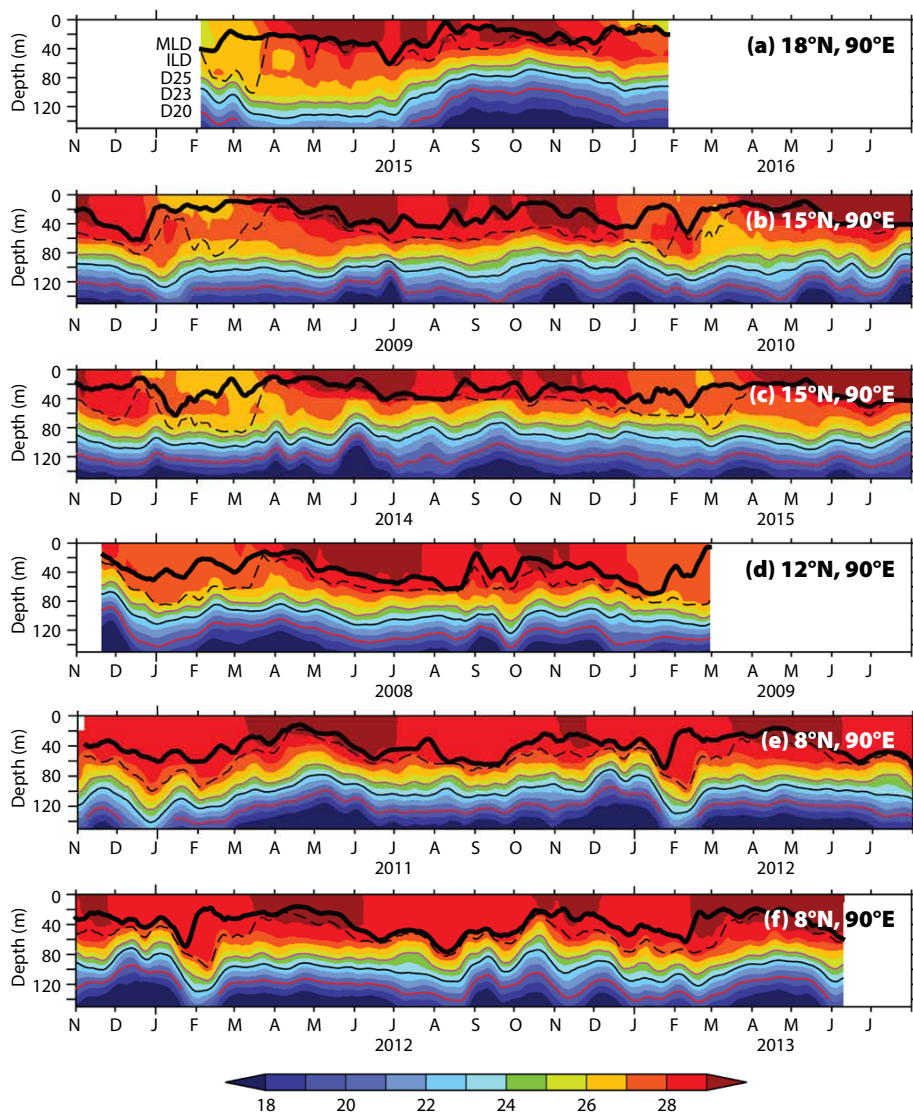


**FIGURE 4.** Temporal evolution of daily temperature (°C) profiles at the buoy locations in the Bay of Bengal. (a) 18°N, 90°E. (b,c) 15°N, 90°E. (d) 12°N, 90°E. (e,f) 8°N, 90°E. Mixed layer depth is indicated by the thick black line, isothermal layer depth by the dashed black line, and depths of the 23°C, 20°C, and 25°C isotherms (D23, D20, D25) by thin black, red, and purple lines, respectively. All of the time series variables are smoothed with a 10-day running mean.



below ML of depths of 10 m, 20 m, and 30 m, respectively.

The residual term includes measurement errors associated with instrumentation, sampling, and parameterization of vertical heat flux processes and penetrating shortwave radiation, and errors associated with finite differencing and missing terms such as horizontal and vertical diffusion (Vialard et al., 2008). All of these calculations are being carried out using daily data that are averaged on seasonal and monthly time scales to perform the subsequent analysis.

## RESULTS AND DISCUSSION

### Seasonal Evolution of SST in the Bay of Bengal

In this section, we discuss the seasonal cycle of the near-surface thermohaline structure in the BoB. Figure 2 shows the seasonal averages of OISST climatology (1997–2015) and their temporal evolution at the mooring locations in the BoB. There is a mild bimodal structure in the evolution of SST in the BoB (Rao and Sivakumar, 2000; Shenoj et al., 2002; Prasad, 2004), with warming from February to mid-May and from mid-August to October, and cooling from November to January and from mid-May to mid-August (Figure 2e). It is interesting to note that warming from February to May is relatively large compared to that from August to October, and the cooling from November to January is higher than that from May to August. In general, temperature gradients are relatively weak from north to south (nearly 0.5°C to 0.7°C) in the BoB except from November to January (Figure 2a), when the north-south temperature contrast reaches as high as 4°C, with a prominent SST minimum occurring in the northern BoB. Moreover, the strongest cooling over a longer duration is observed during winter (November to January) in the northern BoB compared to the south. Furthermore, the comparison between the OISST climatology and buoy SST shows no substantial difference in the seasonal evolution of buoy SST

with respect to the climatological seasonal evolution of SST during the study period (Figure 3). Based on these warming and cooling episodes, the analysis in this study is separated into four seasons: winter (November 1 to January 31), spring (February 1 to May 10), summer (May 11 to August 15), and fall (August 16 to October 31). This definition of seasons is similar to that used by Rao and Sivakumar (2000).

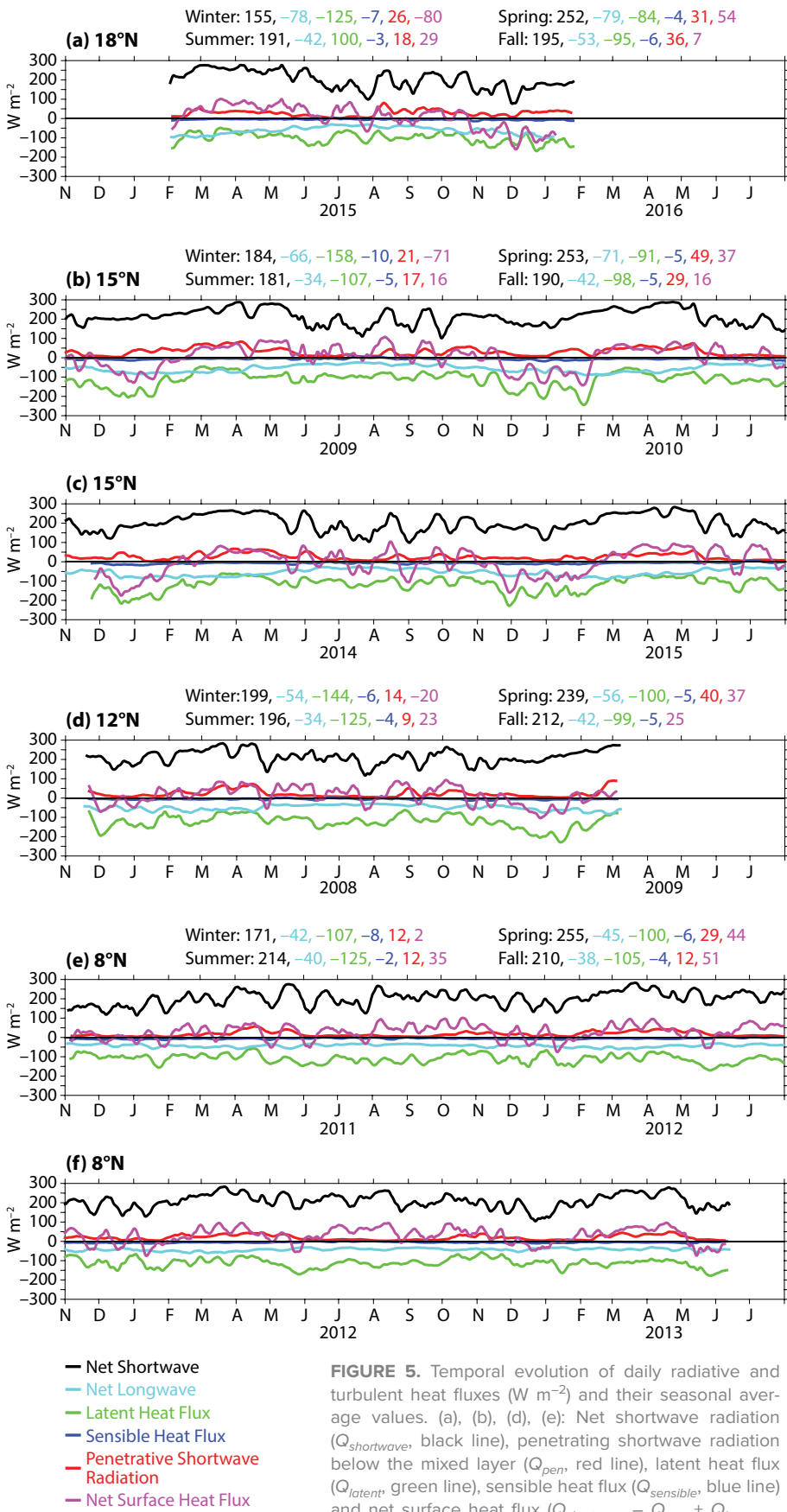
### Seasonal Variability of Latent and Sensible Heat Flux

Figure 5 shows the temporal evolution of radiative and turbulent heat fluxes and their seasonal averages at different buoy locations in the BoB. Figure 6 shows the variability of latent heat flux with respect to near-surface wind speed, relative humidity, and specific humidity difference between sea surface and air at 3 m ( $q_s - q_a$ ). The seasonal averages of wind speed and relative humidity at all of the buoy locations in the BoB are shown in the left and middle columns of Figure 6, respectively. Maximum latent heat loss in the BoB (seasonal average values [SAV] of  $-105 \text{ W m}^{-2}$  to  $-160 \text{ W m}^{-2}$ ) occurs during winter, with the highest loss in the north and decreasing to the south (Figure 5). During the peak of winter, latent heat flux loss from the ocean is as great as  $-300 \text{ W m}^{-2}$  (18°N; Figure 6a). During spring ( $-84$  to  $-100 \text{ W m}^{-2}$ , in SAV) and the summer monsoon (SAVs of  $-100$  to  $-125 \text{ W m}^{-2}$ ), latent heat loss is relatively small compared to winter (Figure 5). During fall, latent heat flux tends to have a clear north (SAV of  $-95 \text{ W m}^{-2}$  at 18°N) to south (SAV of  $-105 \text{ W m}^{-2}$  at 8°N) heat loss trend (Figure 5).

Wind and atmospheric humidity in the near-surface layer primarily determine latent heat losses in the ocean. Although the wind speed is relatively higher ( $6\text{--}12 \text{ m s}^{-1}$ ) during the summer monsoon compared to spring, latent heat losses from the ocean are comparable to spring when lowest wind speeds are observed (Figure 6) because, during

summer, the relative humidity field (80%–90%) is high and uniform throughout the BoB. Hence, during the summer monsoon, the specific humidity difference between the sea surface and the air ( $q_s - q_a$ ) is very small due to the presence of a high-humidity boundary layer in the air that leads to small variability in the latent heat flux ( $-40 \text{ W m}^{-2}$  to  $-120 \text{ W m}^{-2}$ ) with a large range of wind speed ( $3\text{--}12 \text{ m s}^{-1}$ ; Figure 6). This result is consistent with the earlier study by Bhat and Narasimha (2007). They suggested that during the summer monsoon, the dependency of latent heat flux on wind is small in the BoB due to the high humidity. During winter, a clear north-south difference in the humidity fields is observed due to the relatively drier boundary layer air (low relative humidity) in the northern BoB (50%–60%) compared to the southern BoB (70%–80%). Hence, during winter, particularly in the northern BoB, the specific humidity difference between the sea surface and the air directly above it is higher due to the presence of dry boundary-layer air, which leads to large variability in latent heat flux ( $-40 \text{ W m}^{-2}$  to  $-280 \text{ W m}^{-2}$ ), even with a small range of wind speeds ( $4\text{--}8 \text{ m s}^{-1}$ ; Figure 6). Latent heat flux and wind speed show similar relationships, with steep slopes during spring and winter, and gentle slopes during fall and winter. The seasonal variability of the humidity field in the BoB is primarily associated with seasonal variability of the near-surface wind field in the Indian Ocean region. During summer, the large fetch of southwest monsoon winds over the Indian Ocean carries highly humid air into the BoB, and during winter, the northeast wind carries dry continental air into the BoB, reducing the humidity content.

In general, the sensible heat flux is relatively small and reaches its peak during the winter monsoon (SAVs of  $-6 \text{ W m}^{-2}$  to  $-10 \text{ W m}^{-2}$ ) and its minimum during the summer monsoon (SAVs of  $-2$  to  $-5 \text{ W m}^{-2}$ ; Figure 5). During the summer monsoon season, sensible heat flux has positive values (the ocean gains heat)



**FIGURE 5.** Temporal evolution of daily radiative and turbulent heat fluxes ( $\text{W m}^{-2}$ ) and their seasonal average values. (a), (b), (d), (e): Net shortwave radiation ( $Q_{\text{shortwave}}$ ; black line), penetrating shortwave radiation below the mixed layer ( $Q_{\text{pen}}$ ; red line), latent heat flux ( $Q_{\text{latent}}$ ; green line), sensible heat flux ( $Q_{\text{sensible}}$ ; blue line) and net surface heat flux ( $Q_{\text{shortwave}} - Q_{\text{pen}} + Q_{\text{longwave}} + Q_{\text{latent}} + Q_{\text{sensible}}$ ; pink line) at buoy locations (a)  $18^{\circ}\text{N}$ ,  $90^{\circ}\text{E}$ ; (b,c)  $15^{\circ}\text{N}$ ,  $90^{\circ}\text{E}$ ; (d)  $12^{\circ}\text{N}$ ,  $90^{\circ}\text{E}$ ; and (e, f)  $8^{\circ}\text{N}$ ,  $90^{\circ}\text{E}$  in the Bay of Bengal. All of the time series variables are smoothed with 10-day running mean.

occasionally, when the air temperature is higher than SST (Figure 3). Bhat and Fernando (2016, in this issue) examine plausible causative factors for this process.

### Seasonal Variability of Net Shortwave and Net Longwave Radiation and Penetration of Shortwave Radiation Below the Mixed Layer

During winter, the contribution of net shortwave radiation to the ML is reduced significantly ( $155\text{--}200 \text{ W m}^{-2}$ ) over the whole bay; approximately 5%–16 % of shortwave radiation penetrates below the ML, with considerable penetrative loss in the northern BoB, where the ML is shallowest (SAV of 21 m). Similarly, during winter, heat loss from longwave radiation is much larger in the north (SAV of  $-78 \text{ W m}^{-2}$  at  $18^{\circ}\text{N}$ ) and decreases in magnitude to the south (SAV of  $-42 \text{ W m}^{-2}$  at  $8^{\circ}\text{N}$ ); this latitudinal gradient is likely due to variations in the cloud cover (it is cloudier in the south).

During spring, the BoB receives an enormous amount of shortwave radiation compared to other seasons, mainly due to cloudless skies. However, the availability of shortwave radiation decreases from the northern to the southern bay during spring. Although an average of  $225\text{--}253 \text{ W m}^{-2}$  of shortwave radiation is available at the ocean's surface during spring, only a fraction of it (18%; a SAV of approximately  $29\text{--}49 \text{ W m}^{-2}$ ) penetrates below the ML, leaving  $195\text{--}220 \text{ W m}^{-2}$  (SAV) available for the shallow ML (Figure 5), which is shallowest during spring compared to the other seasons. Longwave radiation indicates heat loss from the ocean of  $-45 \text{ W m}^{-2}$  to  $-79 \text{ W m}^{-2}$  (SAV), decreasing from north to south in the BoB in spring (Figure 5).

The intense monsoonal cloud cover during the summer monsoon season leads to a net reduction in shortwave radiation (SAV of  $181\text{--}214 \text{ W m}^{-2}$ ) entering the ocean and longwave radiation (SAV of  $-34$  to  $-42 \text{ W m}^{-2}$ ) leaving the ocean (Figure 5). Relatively less shortwave radiation penetrates below the ML (SAV of



9–18  $W m^{-2}$ , or 5%–10% of net incoming shortwave radiation) during summer due to a deeper MLD and a reduction in incoming shortwave radiation (Figure 5).

During fall, the net shortwave radiation is maximum at 12°N (SAV of 211  $W m^{-2}$ ) and minimum at 15°N (SAV of 190  $W m^{-2}$ ; Figure 5). Similar to spring warming, there is a heat loss in long-wave radiation (SAVs of  $-38 W m^{-2}$  to  $-53 W m^{-2}$ ) from the ocean during fall, with values decreasing from north to south in the BoB (Figure 5).

### Seasonal Variability of the Mixed Layer Heat Budget

Figures 7 and 8 are composites of the temporal evolution of the monthly ML heat budget and the seasonal average of the ML heat budget during selected study periods, respectively. In general, our mixed layer heat budget estimation shows reasonably good agreement with the mixed layer heat storage rate (Figure 7).

#### Winter Cooling

Heat storage in the ML generally declines from north to south in the BoB during winter (November to January), with maximum surface cooling values of  $-53 W m^{-2}$  to  $-10 W m^{-2}$  (Figure 8). The MLD also deepens from north to south, from an average value of 21 m to 42 m (Figure 8). Vertical mixing by moderate winds and convective overturning due to net ocean surface heat loss play active roles in ML deepening (Figure 8; Rao and Sivakumar, 2000; Prasad, 2004; Shroyer et al., 2016, in this issue). Wind speed does not show any significant north-south gradient during winter (Figure 6). Although net surface heat loss is much higher in the northern BoB than in the southern BoB, ML deepening in the northern bay is relatively small compared to that in the southern bay (Figure 8). As suggested by Prasad (2004), the existence of a shallow ML in the northern bay is likely due to strong near-surface salinity stratification, despite the large net surface heat loss. Data from the buoys in the northern BoB show a net surface heat loss as low as  $-150 W m^{-2}$  to

$-175 W m^{-2}$ , a minimum compared to all other seasons (Figure 5b,c). The seasonal average displays an overall decrease in net surface heat loss in the BoB from 18°N ( $-80 W m^{-2}$ ) to 12°N ( $-20 W m^{-2}$ ), with small net surface heat gain at 8°N ( $2 W m^{-2}$ ; Figure 5).

As reported in earlier studies, the barrier layer (temperature inversion) shows maximum thickness (intensity) during winter (Figures 3 and 8; Thadathil et al., 2007; Sengupta et al., 2007; Girishkumar et al., 2011, 2013). The availability of less heat flux in the mixed layer compared to the layer below during winter provide favorable conditions for the formation of

a temperature inversion (Figures 4 and 8; Thadathil et al., 2002; Girishkumar et al., 2013). Though a temperature inversion exists, the vertical density profile is stable due to the presence of strong saline stratification in the near-surface layer (Thadathil et al., 2002).

In the northern BoB, the barrier layer is moderately thick (30–40 m) and there is a strong temperature inversion, whereas in southern BoB both the barrier layer and the temperature inversion are relatively weak and oscillatory in nature (Figure 4; average depth of the barrier layer is 20 m). During winter, the magnitude of the temperature inversion reaches as high as 3°C

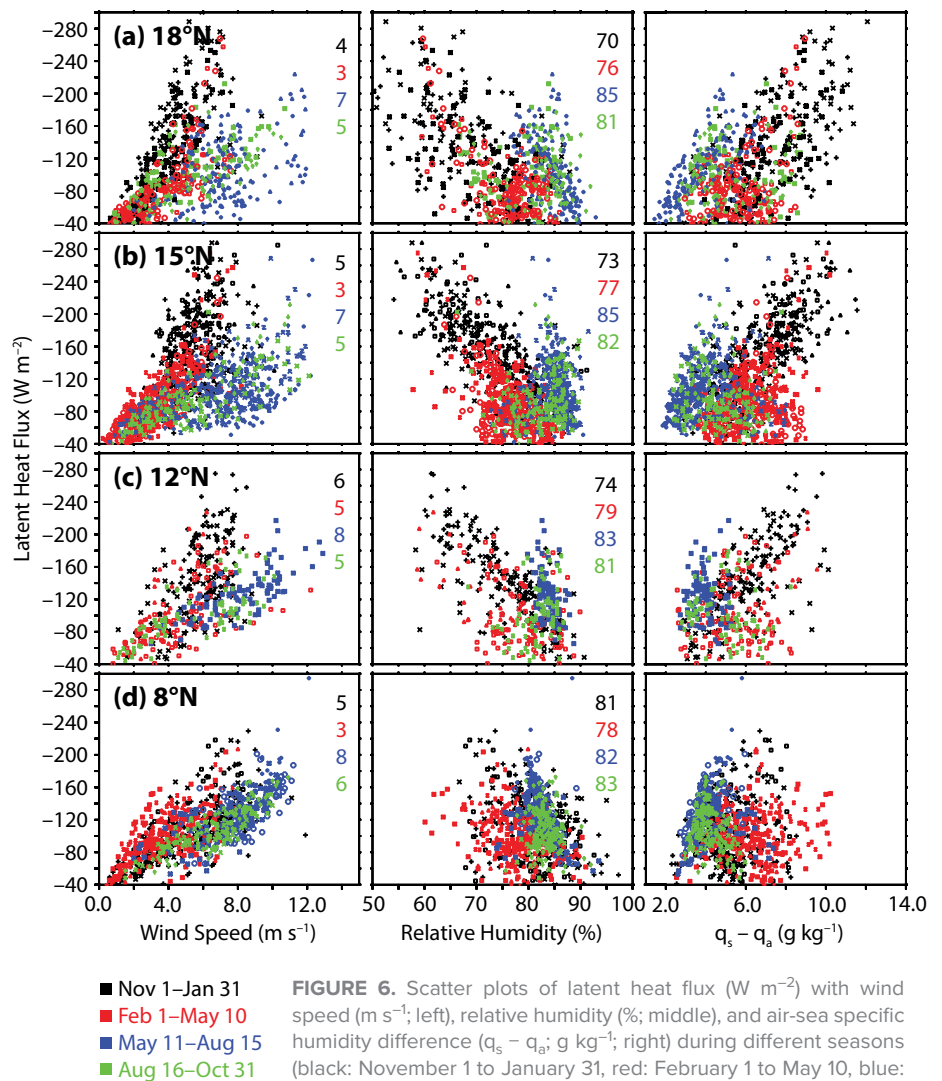


**FIGURE 6.** Scatter plots of latent heat flux ( $W m^{-2}$ ) with wind speed ( $m s^{-1}$ ; left), relative humidity (%; middle), and air-sea specific humidity difference ( $q_s - q_a$ ;  $g kg^{-1}$ ; right) during different seasons (black: November 1 to January 31, red: February 1 to May 10, blue: May 11 to August 15, and green: August 16 to October 31) at buoy locations (a) 18°N, 90°E (WHOI data), (b) 15°N, 90°E, (c) 12°N, 90°E, and (d) 8°N, 90°E in the Bay of Bengal. The numbers in the left and middle panels indicate seasonal (top to bottom: winter, spring, summer, and fall) averages of wind ( $m s^{-1}$ ) and relative humidity (%), respectively, at each buoy location.

in the northern BoB (Figure 3). The magnitude and frequency of the temperature inversion decrease toward the south, primarily due to weaker salinity stratification and relatively smaller differences in net surface heat flux and penetrative short-wave radiation below the ML (Figure 5).

When the barrier layer is thick and temperature inversions exist, vertical mixing of the ML with warm subsurface water can warm and deepen the ML (Figure 4; Sengupta et al., 2007; Boyer Montégut et al., 2007; Girishkumar et al., 2013; Nagura et al., 2015). When a barrier layer exists without a temperature inversion, vertical processes do not significantly contribute to ML temperature variations, due to the small temperature difference between the barrier layer and ML waters (Boyer Montégut et al., 2007; Girishkumar et al., 2013; Nagura et al., 2015). In the northern BoB, vertical

processes contribute to a positive heat flux (SAV of  $41 \text{ W m}^{-2}$  at  $18^\circ\text{N}$ ) into the ML (Figure 8), whereas in the south, vertical processes contribute to a small amount of cooling (SAVs of  $-6 \text{ W m}^{-2}$  at  $12^\circ\text{N}$  to  $-10 \text{ W m}^{-2}$  at  $8^\circ\text{N}$ ) due to the oscillatory nature of the barrier layer and temperature inversion (Figure 8). Although the wind and convective mixing in the near-surface layer are stronger in the southern BoB during winter, the contribution from vertical processes is quite small. This observation suggests that a barrier layer with a temperature inversion can reduce surface cooling even when strong mixing is present.

Horizontal advection contributes to warming at all buoy locations during winter (SAVs vary from  $7 \text{ W m}^{-2}$  to  $24 \text{ W m}^{-2}$  from north to south), and advective heating is comparable to the vertical heat flux at  $15^\circ\text{N}$  (Figure 8). In

the southern BoB, heating by advection is significantly greater than that from vertical processes, which is a loss term. This difference might be associated with the presence of strong zonal and meridional temperature gradients (Figure 2a).

### Spring Warming

During spring, the heat stored in the ML increases significantly from February to May at all buoy locations, though more strongly in the northern BoB ( $52 \text{ W m}^{-2}$  at  $18^\circ\text{N}$ ) compared to the southern BoB ( $18 \text{ W m}^{-2}$  to  $29 \text{ W m}^{-2}$ ; Figure 8). The ML clearly shallows in spring compared to winter, with the MLD reaching as low as 15–20 m during its spring peak (18–28 m, on average; Figures 4 and 8). The ML shallows due to enhancement of near-surface stratification by significant warming of the near-surface layer. This warming is primarily due to the increased net surface heat flux in the presence of low winds ( $<6 \text{ m s}^{-1}$ ). Moreover, the barrier layer and temperature inversion exist during the earlier part of spring but they decrease and even disappear later in the season (Figures 3 and 4). This is primarily due to significant warming of the near-surface layer by surface heat flux that results in the shallowing of the isothermal layer depth (Thadathil et al., 2007; Girishkumar et al., 2011). On average,  $37 \text{ W m}^{-2}$  to  $54 \text{ W m}^{-2}$  net surface heat flux is available to the shallow ML, and it is the most important component of the ML heat budget during spring (50%–60% of the seasonal mean; Figure 5).

Vertical processes do not significantly contribute to the ML heat budget during spring ( $-10 \text{ W m}^{-2}$  to  $-19 \text{ W m}^{-2}$ , explaining 10% of the seasonal mean; Figure 8). Horizontal advection appears to cool the ML somewhat (except at  $18^\circ\text{N}$  and  $8^\circ\text{N}$ ), contributing little to the ML heat budget, possibly due to weaker currents and zonal gradients in temperature (Figure 2b). The other striking characteristic of the ML heat budget during spring is the relatively small value of the residual, which explains 0%–5% of the seasonal mean (Figure 6).

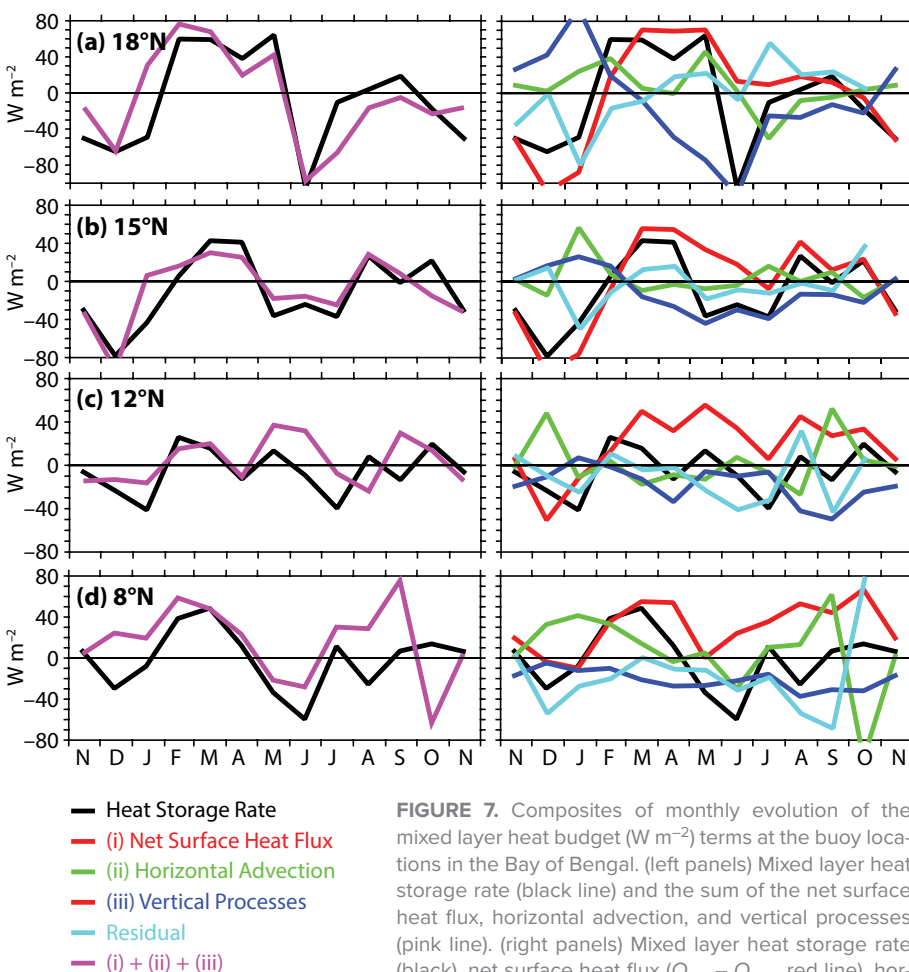


**FIGURE 7.** Composites of monthly evolution of the mixed layer heat budget ( $\text{W m}^{-2}$ ) terms at the buoy locations in the Bay of Bengal. (left panels) Mixed layer heat storage rate (black line) and the sum of the net surface heat flux, horizontal advection, and vertical processes (pink line). (right panels) Mixed layer heat storage rate (black), net surface heat flux ( $Q_{net} - Q_{pen}$ , red line), horizontal advection (green line), vertical processes (blue line), and residual (cyan line).

### Summer Cooling

ML heat storage declines from warming (positive) in spring to cooling (negative) during the summer monsoon season ( $-17 \text{ W m}^{-2}$  to  $-25 \text{ W m}^{-2}$ ), with the highest heat loss in the BoB's interior. In general, the MLD deepens during summer, with a seasonal average MLD around 32–48 m (Figure 8). MLD clearly deepens from north to south, with a maximum depth at 12°N and 8°N (Figure 8). Although the net surface heat flux available to the ML is positive during the summer monsoon season, its magnitude is small compared to that during spring, and there is also less surface warming. Using one-dimensional modeling, Prasad (2004) highlighted the important role that vertical processes

play during summer monsoon cooling due to the presence of moderately strong winds in the BoB. Consistent with the results of Prasad (2004), vertical processes explain 20%–45% of the seasonal mean (Figure 8). The contribution from the horizontal term is weaker during this season and it may be associated with less spatial variation of SST (Figure 2c).

### Fall Warming

During a period of mild warming in fall, the ML shallows a little only in the vicinity of the central BoB buoys ( $8 \text{ W m}^{-2}$  at 15°N and  $19 \text{ W m}^{-2}$  at 12°N; Figure 8). Both the northern and southern buoys do not show any significant trends in temperature. The MLD clearly deepens from north to south during fall (Figures 4 and 8). This

deepening corresponds to an observed decrease in the penetrative component of shortwave radiation from north to south (from  $36 \text{ W m}^{-2}$  at 18°N to  $12 \text{ W m}^{-2}$  at 8°N). Moreover, the barrier layer is much weaker at all the locations in fall compared to spring. Also in fall, a weaker temperature inversion was recorded at all the buoy locations except at 8°N, as compared to spring.

During fall, horizontal advection shows a weak contribution, and vertical processes cool the ML more during this season than in spring. The measured net surface heat flux for fall at all of the buoy locations indicates that the BoB gains heat, with an increasing trend from north ( $7 \text{ m}^{-2}$  at 18°N) to south ( $51 \text{ m}^{-2}$  at 8°N).

### SUMMARY

We sought to quantify the relative contributions of possible factors that modulate the seasonal evolution of SST in the BoB using high-quality in situ observations from a moored buoy network along 90°E. Our analysis of the ML heat budget as a function of the four seasons is consistent with earlier studies. It also suggests

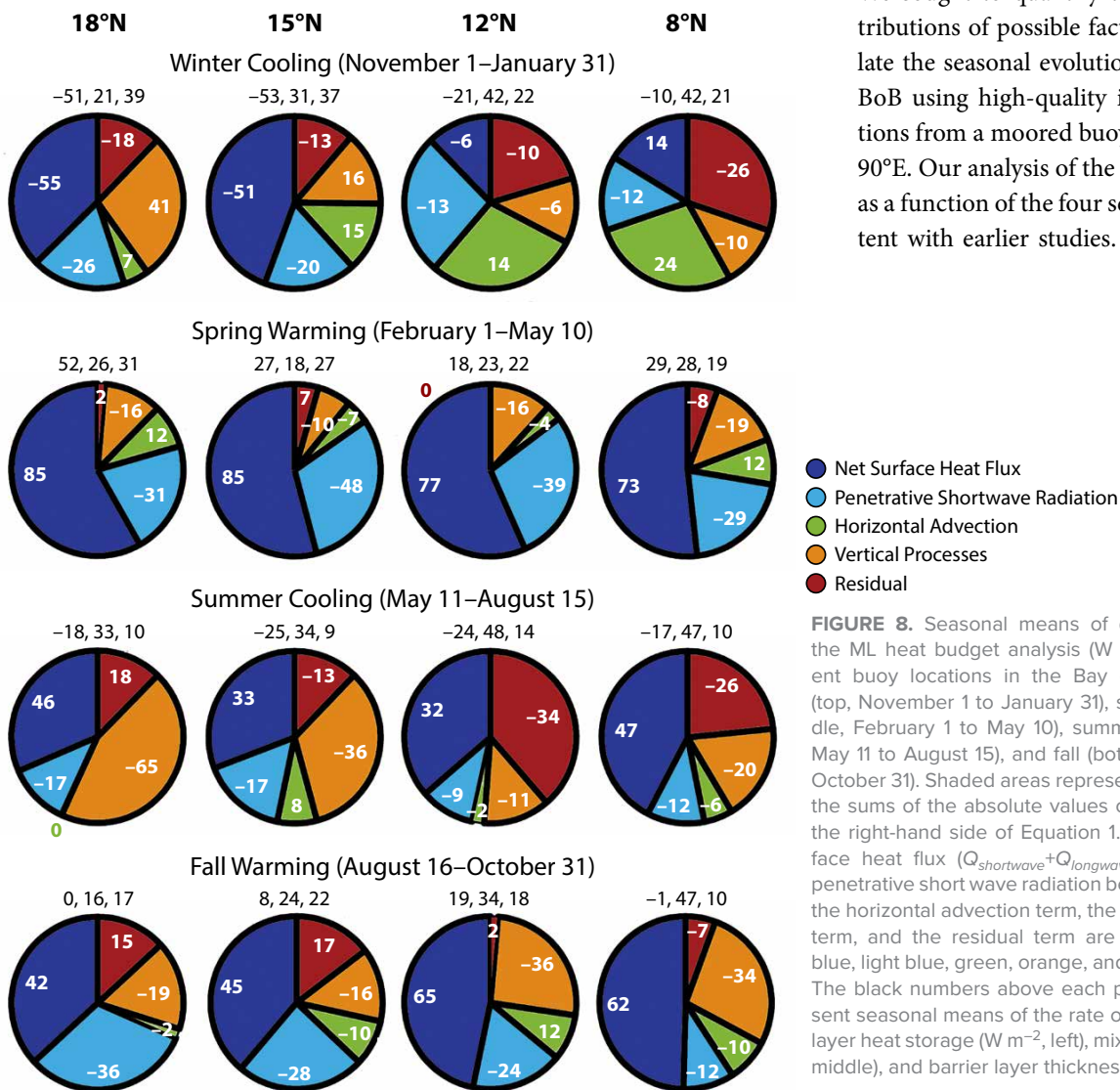


**FIGURE 8.** Seasonal means of different terms of the ML heat budget analysis ( $\text{W m}^{-2}$ ) at the different buoy locations in the Bay of Bengal: winter (top, November 1 to January 31), spring (upper middle, February 1 to May 10), summer (lower middle, May 11 to August 15), and fall (bottom, August 16 to October 31). Shaded areas represent percentages of the sums of the absolute values of all the terms on the right-hand side of Equation 1. The sums of surface heat flux ( $Q_{\text{shortwave}} + Q_{\text{longwave}} + Q_{\text{latent}} + Q_{\text{sensible}}$ ), penetrative short wave radiation below the ML ( $Q_{\text{pen}}$ ), the horizontal advection term, the vertical processes term, and the residual term are indicated in dark blue, light blue, green, orange, and red, respectively. The black numbers above each pie diagram represent seasonal means of the rate of change of mixed layer heat storage ( $\text{W m}^{-2}$ , left), mixed layer depth (m, middle), and barrier layer thickness (m, right).



that although net surface heat flux is the primary factor in determining the seasonal variation of SST in the BoB, ocean dynamics also plays a crucial role (Rao and Sivakumar, 2000; Sengupta et al., 2002; Shenoj et al., 2002; Prasad, 2004; Boyer Montégut et al., 2007; Parampil et al., 2010; Girishkumar et al., 2013; Nagura et al., 2015).

During the winter cooling period, a reduction in surface heat flux leads to a decrease in ML temperature, with maximum cooling in the northern BoB. Our study shows that horizontal advection has a warming tendency, though it contributes only 10%–30% to the ML heat budget, consistent with earlier work by Parampil et al. (2010) and Nagura et al. (2015). Another key factor affecting the ML heat budget is the presence of a strong barrier layer, especially in winter. Nagura et al. (2015) and Boyer Montégut et al. (2007) showed that during winter, the barrier layer supports strong temperature inversions; hence, the vertical process term in Equation 1 indicates warming, particularly in the northern BoB. In this study, this warming signature is evident at 15°N; approximately 16 W m<sup>-2</sup> of heat is added to the ML by vertical entrainment of warm water. In the southern BoB, where the temperature inversion and the barrier layer occur during winter, the vertical heat flux term in Equation 1 is approximated to -6 W m<sup>-2</sup> to -20 W m<sup>-2</sup> and is in good agreement with earlier results of Girishkumar et al. (2013), which show that nearly -10 W m<sup>-2</sup> to -20 W m<sup>-2</sup> heat enters the ML by vertical entrainment.


During the spring warming period, the ML temperature balance is predominantly controlled by net surface heat flux and penetrative shortwave radiation below the ML, and accounts for 72%–85% of ML temperature variability. Due to the presence of a shallow ML and availability of more shortwave radiation, penetrative radiation reaches its maximum during spring (30–50 W m<sup>-2</sup>), and it is comparable in magnitude (45 W m<sup>-2</sup>) with that from earlier studies by Sengupta et al. (2002) and Boyer Montégut et al. (2007).

Parampil et al. (2010) suggested that horizontal advection might play an important role in the ML heat budget during spring. Though the magnitude of horizontal advection in spring is comparable with that of winter, its contribution to the ML heat budget is relatively small during spring.

During summer, the reduction in net surface heat flux leads to mild ML cooling. Consistent with the results of Prasad (2004) and Neethu et al. (2012), vertical heat flux plays an important role in the ML heat budget, which explains 20%–45% of the seasonal mean. As suggested by Parampil et al. (2010), the contribution from horizontal advection is relatively weak during summer, and it is associated with relatively less spatial variation in SST.

The seasonal variation of humidity plays an important role in modulating the latent heat flux in the BoB. During winter, the presence of a relatively dry boundary layer of air (relative humidity is nearly 70%), particularly in the northern BoB, leads to large variability in latent heat flux (-40 W m<sup>-2</sup> to -240 W m<sup>-2</sup>) with respect to a small wind speed range (4–8 m s<sup>-1</sup>). During summer, the humidity field is relatively high (relative humidity is nearly 80%–90%) and uniform throughout the BoB and latent heat flux varies between -40 W m<sup>-2</sup> and -120 W m<sup>-2</sup> with respect to a relatively large wind speed range (3–12 m s<sup>-1</sup>).

It is interesting to note that the contribution of the residual term in Equation 1 to the ML heat budget is relatively large during the cooling phase (Figure 6) compared to the warming phase when the contribution from vertical heat flux plays a significant role. It indicates that vertical mixing may play an important role in the ML heat budget during the cooling period. The availability of high-quality turbulent measurements in the upper ocean may provide valuable insight into the seasonal variability of vertical mixing in the BoB (Warner et al. and Shroyer et al., 2016, both in this issue). Further, the role of submesoscale processes in modulating

the seasonal variability of SST in the BoB needs to be explored. The availability of high-resolution spatiotemporal hydrographic and  $\chi$ pod data from moorings collected during the Ocean Mixing and Monsoon (OMM) program and Air-Sea Interactions Regional Initiative (ASIRI) may provide an opportunity to directly estimate the contributions of horizontal advection, subsurface turbulent heat fluxes, and submesoscale processes to the evolution of SST in the BoB (Warner et al., 2016, in this issue). 

## REFERENCES

- Bhat, G.S., and H.J.S. Fernando. 2016. Remotely driven anomalous sea-air heat flux over the north Indian Ocean during the summer monsoon season. *Oceanography* 29(2):232–241, <http://dx.doi.org/10.5670/oceanog.2016.55>.
- Bhat, G.S., and R. Narasimha. 2007. Indian summer monsoon experiments. *Current Science* 93(2):153–164.
- Boyer Montégut, C., J. Vialard, S.S.C. Shenoj, D. Shankar, F. Durand, C. Ethé, and G. Madec. 2007. Simulated seasonal and interannual variability of mixed layer heat budget in the northern Indian Ocean. *Journal of Climate* 20:3,249–3,268, <http://dx.doi.org/10.1175/JCLI4148.1>.
- Chowdary, J.S., A. Parekh, S. Ojha, and C. Gnanaseelan. 2015. Role of upper ocean processes in the seasonal SST evolution over tropical Indian Ocean in climate forecasting system. *Climate Dynamics* 45:2,387–2,405, <http://dx.doi.org/10.1007/s00382-015-2478-4>.
- Dickey, T.D., D.V. Manov, R.A. Weller, and D.A. Siegel. 1994. Determination of longwave heat flux at the air-sea interface using measurements from buoy platforms. *Journal of Atmospheric and Oceanic Technology* 11(4):1,057–1,078, [http://dx.doi.org/10.1175/1520-0426\(1994\)011<1057:DOLHFA>2.0.CO;2](http://dx.doi.org/10.1175/1520-0426(1994)011<1057:DOLHFA>2.0.CO;2).
- Du, Y., T. Qu, G. Meyers, Y. Masumoto, and H. Sasaki. 2005. Seasonal heat budget in the mixed layer of the southeastern tropical Indian Ocean in a high-resolution ocean general circulation model. *Journal of Geophysical Research* 110, C04012, <http://dx.doi.org/10.1029/2004JC002845>.
- Fairall, C.W., E.F. Bradley, J.E. Hare, A.A. Grachev, and J.B. Edson. 2003. Bulk parameterization of air-sea fluxes: Updates and verification for the COARE algorithm. *Journal of Climate* 16:571–591, [http://dx.doi.org/10.1175/1520-0442\(2003\)016<0571:BPOASF>2.0.CO;2](http://dx.doi.org/10.1175/1520-0442(2003)016<0571:BPOASF>2.0.CO;2).
- Gentemann, C., C.J. Donlon, A. Stuart-Menteth, and F.J. Wentz. 2003. Diurnal signals in satellite sea surface temperature measurements. *Geophysical Research Letters* 30(3):1,140–1,143, <http://dx.doi.org/10.1029/2002GL016291>.
- Girishkumar, M.S., M. Ravichandran, and M.J. McPhaden. 2013. Temperature inversions and their influence on the mixed layer heat budget during the winters of 2006–2007 and 2007–2008 in the Bay of Bengal. *Journal of Geophysical Research* 118:2,426–2,437, <http://dx.doi.org/10.1002/jgrc.20192>.
- Girishkumar, M.S., M. Ravichandran, M.J. McPhaden, and R.R. Rao. 2011. Intraseasonal variability in barrier layer thickness in the south central BoB. *Journal of Geophysical Research* 116, C03009, <http://dx.doi.org/10.1029/2010JC006657>.
- Kara, A.B., P.A. Rochford, and H.E. Hurlbutt. 2000. Mixed layer depth variability and barrier layer formation over the North Pacific Ocean. *Journal of Geophysical Research* 105(C7):16,783–16,801, <http://dx.doi.org/10.1029/2000JC900071>.

- Lukas, R., and E. Lindstrom. 1991. The mixed layer of the western equatorial Pacific Ocean. *Journal of Geophysical Research* 96:3,343–3,357, <http://dx.doi.org/10.1029/90JC01951>.
- McPhaden, M.J. 1982. Variability in the central equatorial Indian Ocean: Part II. Oceanic heat and turbulent energy balance. *Journal of Marine Research* 40:403–419.
- McPhaden, M.J., G. Meyers, K. Ando, Y. Masumoto, V.S.N. Murty, M. Ravichandran, F. Syamsudin, J. Vialard, L. Yu, and W. Yu. 2009. RAMA, The Research Moored Array for African–Asian–Australian Monsoon Analysis and Prediction: A new moored buoy array in the historically data-sparse Indian Ocean provides measurements to advance monsoon research and forecasting. *Bulletin of the American Meteorological Society* 90:459–480, <http://dx.doi.org/10.1175/2008BAMS2608.1>.
- Morel, A. 1988. Optical modeling of the upper ocean in relation to its biogenous matter content (case I waters). *Journal of Geophysical Research* 93:1,652–1,665, <http://dx.doi.org/10.1029/JC093iC09p10749>.
- Nagura, M., T. Terao, and M. Hashizume. 2015. The role of temperature inversions in the generation of seasonal and interannual SST variability in the far northern Bay of Bengal. *Journal of Climate* 28:3,671–3,693, <http://dx.doi.org/10.1175/JCLI-D-14-00553.1>.
- Neethu, C., M. Ravichandran, R.R. Rao, and S.S.C. Shenoi. 2012. An anomalous cooling event observed in the Bay of Bengal during June 2009. *Ocean Dynamics* 62(5):671–681, <http://dx.doi.org/10.1007/s10236-012-0525-9>.
- Palmer, T.N., and D.A. Mansfield. 1984. Response of two atmospheric general circulation models to sea-surface temperature anomalies in the tropical east and west Pacific. *Nature* 310:483–488, <http://dx.doi.org/10.1038/310483a0>.
- Parampil, S.R., A. Gera, M. Ravichandran, and D. Sengupta. 2010. Intraseasonal response of mixed layer temperature and salinity in the Bay of Bengal to heat and freshwater flux. *Journal of Geophysical Research* 115, C05002, <http://dx.doi.org/10.1029/2009JC005790>.
- Prasad, T.G. 2004. A comparison of mixed-layer dynamics between the Arabian Sea and Bay of Bengal: One-dimensional model results. *Journal of Geophysical Research* 109, C03035, <http://dx.doi.org/10.1029/2003JC002000>.
- Praveen Kumar, B., J. Vialard, M. Lengaigne, V.S.N. Murty, and M.J. McPhaden. 2012. TropFlux: Air-sea fluxes for the global tropical oceans—description and evaluation. *Climate Dynamics* 38:1,521–1,543, <http://dx.doi.org/10.1007/s00382-011-1115-0>.
- Rao, R.R., and R. Sivakumar. 2000. Seasonal variability of near-surface thermal structure and heat budget of the mixed layer of the tropical Indian Ocean from a new global ocean temperature climatology. *Journal of Geophysical Research* 105(C1):995–1,016, <http://dx.doi.org/10.1029/1999JC900220>.
- Rao, R.R., and R. Sivakumar. 2003. Seasonal variability of sea surface salinity and salt budget of the mixed layer of the north Indian Ocean. *Journal of Geophysical Research* 108(C1), 3009, <http://dx.doi.org/10.1029/2001JC000907>.
- Sengupta, D., B.R. Goddalahundi, and D.S. Anitha. 2007. Cyclone-induced mixing does not cool SST in the post-monsoon North Bay of Bengal. *Atmospheric Science Letters* 9:1–6, <http://dx.doi.org/10.1002/asl.162>.
- Sengupta, D., B.N. Goswami, and R. Senan. 2001. Coherent intraseasonal oscillations of ocean and atmosphere during the Asian summer monsoon. *Geophysical Research Letters* 28(21):4127–4130, <http://dx.doi.org/10.1029/2001GL013587>.
- Sengupta, D., and M. Ravichandran. 2001. Oscillations in the Bay of Bengal sea surface temperature during the 1998 summer monsoon. *Geophysical Research Letters* 28:2,033–2,036, <http://dx.doi.org/10.1029/2000GL012548>.
- Sengupta, D., P.K. Ray, and G.S. Bhat. 2002. Spring warming of the eastern Arabian Sea and Bay of Bengal from buoy data. *Geophysical Research Letters* 29(15), <http://dx.doi.org/10.1029/2002GL015340>.
- Sharmila, S., P.A. Pillai, S. Joseph, M. Roxy, R.P.M. Krishna, R. Chattopadhyay, S. Abhilash, A.K. Sahai, and B.N. Goswami. 2013. Role of ocean–atmosphere interaction on northward propagation of Indian summer monsoon intra-seasonal oscillations (MISO). *Climate Dynamics* 41(5):1,651–1,669, <http://dx.doi.org/10.1007/s00382-013-1854-1>.
- Shenoi, S.S.C., D. Shankar, and S.R. Shetye. 2002. Differences in heat budgets of the near-surface Arabian Sea and Bay of Bengal: Implications for the summer monsoon. *Journal of Geophysical Research* 107(C6), <http://dx.doi.org/10.1029/2000JC000679>.
- Shetye, S.R., A.D. Gouveia, D. Shankar, S.S.C. Shenoi, P. Vinayachandran, N. Sundar, G.S. Michael, and G. Namboodiri. 1996. Hydrography and circulation in the western Bay of Bengal during the northeast monsoon. *Journal of Geophysical Research* 101(6):14,011–14,025, <http://dx.doi.org/10.1029/95JC03307>.
- Shroyer, E.L., D.L. Rudnick, J.T. Farrar, B. Lim, S.K. Venayagamoorthy, L.C. St. Laurent, A. Garanaik, and J.N. Moum. 2016. Modification of upper-ocean temperature structure by subsurface mixing in the presence of strong salinity stratification. *Oceanography* 29(2):62–71, <http://dx.doi.org/10.5670/oceanog.2016.39>.
- Sprintall, J., and M. Tomczak. 1992. Evidence of the barrier layer in the surface layer of the tropics. *Journal of Geophysical Research* 97:7,305–7,316, <http://dx.doi.org/10.1029/92JC00407>.
- Thadathil, P., V.V. Gopalakrishna, P.M. Muraliedharan, G.V. Reddy, N. Araligidad, and S. Shenoy. 2002. Surface layer temperature inversion in the Bay of Bengal. *Deep Sea Research Part I* (49):1,801–1,818, [http://dx.doi.org/10.1016/S0967-0637\(02\)00044-4](http://dx.doi.org/10.1016/S0967-0637(02)00044-4).
- Thadathil, P., P.M. Muraliedharan, R.R. Rao, Y.K. Somayajulu, G.V. Reddy, and C. Revichandran. 2007. Observed seasonal variability of barrier layer in the Bay of Bengal. *Journal of Geophysical Research* 112, C02009, <http://dx.doi.org/10.1029/2006JC003651>.
- Venkatesan, R., V.R. Shamji, G. Latha, S. Mathew, R.R. Rao, A. Muthiah, and M.A. Atmanand. 2013. In situ ocean subsurface time-series measurements from OMNI buoy network in the Bay of Bengal. *Current Science* 104:1,166–1,177.
- Vialard, J., G.R. Foltz, M.J. McPhaden, J.P. Duvel, and C. de Boyer Montégut. 2008. Strong Indian Ocean sea surface temperature signals associated with the Madden-Julian Oscillation in late 2007 and early 2008. *Geophysical Research Letters* 35, L19608, <http://dx.doi.org/10.1029/2008GL035238>.
- Warner, S.J., J. Becherer, K. Pujiana, E.L. Shroyer, M. Ravichandran, V.P. Thangaprakash, and J.N. Moum. 2016. Monsoon mixing cycles in the Bay of Bengal: A year-long subsurface mixing record. *Oceanography* 29(2):158–169, <http://dx.doi.org/10.5670/oceanog.2016.48>.

and cooperation. This work was supported by MoES under the National Monsoon Mission, Ocean Mixing and Monsoon (OMM) program. This is INCOIS publication no. 257.

## AUTHORS

V.P. Thangaprakash (vptincois@gmail.com), M.S. Girishkumar, K. Suprit, and N. Suresh Kumar are all scientists at the Indian National Centre for Ocean Information Services, Hyderabad, India. Dipanjan Chaudhuri is a graduate student at the Centre for Atmospheric and Oceanic Sciences, Indian Institute of Science, Bangalore, India. K. Dinesh is a scientific assistant, Ashok Kumar is Project Assistant, S. Shivaprasad is Scientist, and M. Ravichandran is Head, Observations and Modeling, Indian National Centre for Ocean Information Services, Hyderabad, India. J. Thomas Farrar is Associate Scientist, Woods Hole Oceanographic Institution, Woods Hole, MA, USA. R. Sundar is a scientist at the National Institute of Ocean Technology, Chennai, India. Robert A. Weller is Senior Scientist, Woods Hole Oceanographic Institution, Woods Hole, MA, USA.

## ARTICLE CITATION

Thangaprakash, V.P., M.S. Girishkumar, K. Suprit, N. Suresh Kumar, D. Chaudhuri, K. Dinesh, A. Kumar, S. Shivaprasad, M. Ravichandran, J.T. Farrar, R. Sundar, and R.A. Weller. 2016. What controls seasonal evolution of sea surface temperature in the Bay of Bengal? Mixed layer heat budget analysis using moored buoy observations along 90°E. *Oceanography* 29(2):202–213, <http://dx.doi.org/10.5670/oceanog.2016.52>.

## ACKNOWLEDGMENTS

The encouragement and facilities provided by the Director of the Indian National Center for Ocean Information Services (INCOIS), Hyderabad, India, are gratefully acknowledged. RAMA data are provided by the TAO Project Office of NOAA/PMEL. OMNI buoys are deployed and maintained by ESSO-NIOT and data are provided by ESSO-INCOIS. We thank Amy Waterhouse, SIO, USA, and all anonymous reviewers who helped us to improve our manuscript. The WHOI buoy deployment was supported by the US Office of Naval Research (grant no. N00014-13-10453). We thank Jothilingam and Rohith (both at INCOIS) for their help in improving the quality of figures. We would like to extend our thanks to all guest editors and the editor for their great support